# Correction of optical phase aberrations using binary-amplitude modulation

**Tom Vettenburg and Andy R. Harvey***

*School of Engineering and Physical Sciences, Heriot-Watt University, Edinburgh EH14 4AS, UK*
**Corresponding author: a.r.harvey@hw.ac.uk*

Received October 27, 2010; revised December 22, 2010; accepted December 25, 2010;
posted January 10, 2011 (Doc. ID 137255); published MONTH 0, 0000

We show that phase aberrations in an imaging system can be mitigated using binary-amplitude masks that reduce destructive interference in the image spatial frequency domain. Appropriately designed masks increase the magnitude of the optical transfer function and prevent nulls. This offers a low-cost, transmission-mode alternative to phase correction as used in active and adaptive optics, without a restriction on the waveband of operation. 

*OCIS codes:* 070.0070, 110.0110, 110.1758, 010.1080, 110.0115, 070.6120.

## 1. INTRODUCTION

We describe a new approach employing pupil-plane binary-amplitude masks for the mitigation of phase aberrations in imaging. Although the pupil phase can be corrected using active or adaptive optics [1–3], wavefront modulators tend to be expensive and the necessary reflection geometry can be a disadvantage. Low-cost, transmissive, liquid-crystal phase modulation, on the other hand, is limited to use at visible and near-infrared wavelengths. Binary phase modulation using ferroelectric liquid crystals has been considered as an alternative to continuous modulation [4]; however, binary-amplitude modulation offers lower complexity and cost, and it can be accomplished efficiently from ultraviolet to far-infrared wavelengths with a wide variety of fixed or agile spatial-light amplitude-modulation techniques [5–8]. We show that a binary-amplitude mask located at the aperture stop can be optimized to mitigate phase aberrations and allow sufficient information to be recorded for the recovery of a sharp image using standard digital-image restoration.

We derive an upper limit for the asymptotic modulation-transfer function (MTF) obtainable in the presence of large aberrations, using binary-amplitude masks in general. Although a mask could be devised to yield the asymptotic MTF for specific spatial frequencies, it is unlikely that masks exist that approach the limit at all spatial frequencies simultaneously. However, significant image contrast across all spatial frequencies is obtained for masks that selectively block destructively interfering parts of the aperture, and such a mask can be considered to be the amplitude mask equivalent of the phase mask proposed by Love *et al.* [9,10]. Here we derive an analytical expression for the MTF when masking arbitrarily large aberrations, which can be seen to be in agreement with the Strehl ratio found for the phase mask in [9]. Furthermore, we show that for aberrations as large as 3.5 waves of root-mean-square optical path difference, part of the MTF can be increased beyond the asymptotic limit by optimization of three additional free parameters of the mask. More recently, a similar binary-amplitude modulation has been suggested for the correction of residual aberrations in adaptive optics by Osborn *et al.* [11]. Rigorous simulations showed that the contrast can be improved significantly by selectively blocking areas of the pupil where the wavefront aberration surpassed a chosen threshold. Sufficient mask transmission is maintained because the residual aberrations are relatively modest. In contrast, the technique described here enables high optical transmission for arbitrarily high aberrations.

In the following section, the asymptotic MTF is derived for large aberrations and for binary-amplitude masks in general. In Section 3, contour masks are introduced, and an analytical expression is derived for their MTF. Performance in the presence of common aberrations is evaluated for paraxial imaging with monochromatic light, and it is found to be in close agreement with the derived MTF; however, some improvement over the asymptotic case was obtained by optimization of the free parameters of the mask. Finally, the contour mask is evaluated for off-axis imaging with a compound lens in broadband light. Although the contrast is lower than that predicted for monochromatic illumination, the resultant contrast is deemed sufficient to enable digital image recovery for this lens.

## 2. CONTRAST OBTAINABLE IN THE PRESENCE OF LARGE ABERRATIONS

The influence of an aberrations on the optical transfer function (OTF) of an optical system can be lucidly understood from the autocorrelation of the pupil function [12]:

$$\mathrm{OTF}(\boldsymbol{\nu}) = \frac{1}{\mathrm{supp}(P)} \iint P^*(\mathbf{u}-\boldsymbol{\nu})P(\mathbf{u}+\boldsymbol{\nu})\mathrm{d}\mathbf{u}, \qquad (1)$$

with the pupil function being $P(\mathbf{u}) = \exp(il(\mathbf{u}))$, $\forall\ \mathbf{u}\|\mathbf{u}\| \le 1$, and 0 otherwise; where $l(\mathbf{u})$ is the optical path length variation expressed in radians; while $\mathbf{u}$ and $\boldsymbol{\nu}$ are the normalized pupil coordinate and spatial frequency, respectively. The OTF is normalized by division by $\mathrm{supp}(P)$, the support of the pupil function, equal to $\pi$ for a circular aperture. For our purpose Eq. (1) can be simplified to

 

$$\mathrm{OTF}(\boldsymbol{\nu}) = \frac{1}{\mathrm{supp}(P)} \iint_{\Omega(\boldsymbol{\nu})} \exp(i\Delta(\mathbf{u},\boldsymbol{\nu}))\mathrm{d}\mathbf{u}, \tag{2}$$

where $\Delta(\mathbf{u},\boldsymbol{\nu}) = l(\mathbf{u}+\boldsymbol{\nu}) - l(\mathbf{u}-\boldsymbol{\nu})$, is the difference in the optical path length between two points on the pupil $2\boldsymbol{\nu}$ apart and $\Omega(\boldsymbol{\nu})$ is the integration region of the autocorrelated pupil.

It is informative to decompose the integrand in Eq. (2) by plotting definite integrals with increasing limit in the complex plane [13], as depicted in Fig. 1, for a circular aperture for $\|\boldsymbol{\nu}\| = 1/2$. In the case of a modest defocus of $W_{20} = \lambda/4$, then $-\pi/2 \le \Delta(\mathbf{u},\boldsymbol{\nu}) \le \pi/2$, as can be seen from the slope of the curve in Fig. 1(a), and all components contribute constructively to the resultant phasor. For larger aberrations, a destructive interference contributes to the resultant phasor and leads to a reduced MTF, or nulls as shown in Fig. 1(b). By devising an appropriate pupil mask, we aim to avoid excessive suppression of the MTF by removing or reducing those destructive contributions, as depicted in Fig. 1(c). We will show that in the presence of large aberrations, sufficiently high contrast can be guaranteed to enable the digital recovery of a high-quality image.

The MTF with binary mask $M(\mathbf{u}) \in \{0,1\}$, can be calculated for large aberrations for which $\Delta(\mathbf{u},\boldsymbol{\nu})\mathrm{mod}2\pi$ in Eq. (2) can be considered to be uniformly distributed in the interval $[0,2\pi]$. The ideal mask would permit only constructive interference for constituent image phasors, i.e., for $(\Delta(\mathbf{u},\boldsymbol{\nu}) + \pi/2)\mathrm{mod}2\pi \le \pi$. Assuming that the ideal mask exists, in general for $\|\boldsymbol{\nu}\| > 0$, the double integral in Eq. (2) can be written as a single-dimensional Lebesgue integral [14], and approximated as shown in Appendix A for large aberrations by

$$\begin{aligned}\mathrm{OTF}_i(\boldsymbol{\nu}) &= \frac{1}{\mathrm{supp}(P)}\frac{1}{T}\int_{-\frac{\pi}{2}}^{\frac{\pi}{2}} \exp(i\Delta)\mu'(\boldsymbol{\nu},\Delta)\mathrm{d}\Delta \\ &\approx \frac{1}{\mathrm{supp}(P)}\frac{1}{T}\frac{A_\Omega(\boldsymbol{\nu})}{2\pi}\int_{-\frac{\pi}{2}}^{\frac{\pi}{2}} \exp(i\Delta)\mathrm{d}\Delta,\end{aligned} \tag{3}$$

where, in the limit for large aberrations, $\mu'(\boldsymbol{\nu},\Delta) = A_\Omega(\boldsymbol{\nu})/2\pi$ accounts for the change in integration variables and $1/T$ renormalizes the transfer function for a mask with transmission, $T$. The area of overlap of the autocorrelated pupil function, $A_\Omega(\boldsymbol{\nu})$, at spatial frequency $\boldsymbol{\nu}$, is equal to the product of the area of support of the pupil function, $\mathrm{supp}(P)$, and the diffraction-limited MTF at $\boldsymbol{\nu}$, $\mathrm{MTF}_{\mathrm{DL}}(\boldsymbol{\nu})$. Considering also that $T \to 1/2$ for large aberrations, the upper limit of the MTF with the putative amplitude mask is given by

$$\mathrm{MTF}_p(\boldsymbol{\nu}) \approx \frac{2}{\pi}\mathrm{MTF}_{\mathrm{DL}}(\boldsymbol{\nu}) \approx 0.64\mathrm{MTF}_{\mathrm{DL}}(\boldsymbol{\nu}). \tag{4}$$

For a specific spatial frequency $\|\boldsymbol{\nu}\| \ge 1/2$, it is straightforward to find a mask satisfying Eq. (4); however, for a broad range of spatial frequencies and an arbitrary aberration, such a mask might not exist. The optimal mask can be found by a rigorous search over a high-dimensional discretized mask space [15]. Although such an approach is practical when the aberration and optimal mask are fixed, for dynamic aberrations requiring an adaptive optimization of masks, the computational burden for this approach is probably too great for most real-time applications. We show in Section 3 how the optimization can be confined to the more tractable three-dimensional space of the contour masks.

## 3. CONTOUR MASKS

We propose here the use of contour masks for general aberrations, because they yield comparable contrast to discretized masks, but require only low-dimensional global optimization. We define the contour mask, $M(\mathbf{u})$, for an aberration characterized by an optical path length variation, $l(\mathbf{u})$, as

$$M(\mathbf{u}) = 1, \forall\ \mathbf{u} \left| \left( l(\mathbf{u}) - \varphi_0 - \mathbf{t}\cdot\mathbf{u} + \frac{\Delta\varphi}{2} \right) \mathrm{mod}2\pi \le \Delta\varphi, \right. \tag{5}$$

where $\Delta\varphi$ is the maximum permitted phase difference between any two points in the pupil. The to-be-optimized parameters $\varphi_0$ and $\mathbf{t}$ are the reference phase and the tip-tilt, respectively. In the simple case of defocus, $M(\mathbf{u})$ is a Fresnel zone plate. The introduction of tip-tilt, $\mathbf{t}$, merely displaces the imaged field of view. For modest displacements, such imaging systems can be considered equivalent; hence, tip-tilt is included as an additional free parameter in the optimization process, potentially improving the contrast further.

### A. Contrast for Monochromatic Illumination

More generally, and for sufficiently large aberrations, the pupil phase, $\varphi(\mathbf{u}) = l(\mathbf{u})\mathrm{mod}2\pi$ can be considered to be uniformly distributed in the interval $[0,2\pi]$, and for $\|\boldsymbol{\nu}\| > 0$, the phases $\varphi_1 = \varphi(\mathbf{u}-\boldsymbol{\nu})$ and $\varphi_2 = \varphi(\mathbf{u}+\boldsymbol{\nu})$ are independent, so that the integral in Eq. (2) can be approximated as follows:

$$\mathrm{OTF}(\boldsymbol{\nu}) \approx \frac{\mathrm{MTF}_{\mathrm{DL}}(\boldsymbol{\nu})}{4\pi^2}\int_{-\pi}^{\pi}\exp(-i\varphi_1)\int_{-\pi}^{\pi}\exp(i\varphi_2)\mathrm{d}\varphi_2\mathrm{d}\varphi_1, \tag{6}$$

where the factor $\mathrm{MTF}_{\mathrm{DL}}(\boldsymbol{\nu})/4\pi^2$ accounts for the change in integration variables as, demonstrated in Appendix B. The integrals evaluate to zero, as expected for large aberrations. Contour masks, on the other hand, permit only interference of phases $-\Delta\varphi/2 \le l(\mathbf{u})\mathrm{mod}2\pi \le \Delta\varphi/2$, so that the OTF can be calculated by changing the integration limits in Eq. (6) to give a contour mask OTF without nulls:

$$\mathrm{OTF}_c(\boldsymbol{\nu}) \approx \frac{2\pi}{\Delta\varphi}\frac{\mathrm{MTF}_{\mathrm{DL}}(\boldsymbol{\nu})}{\pi^2}\sin^2\left(\frac{\Delta\varphi}{2}\right) \le \frac{2}{\pi^2}\mathrm{MTF}_{\mathrm{DL}}(\boldsymbol{\nu}). \tag{7}$$

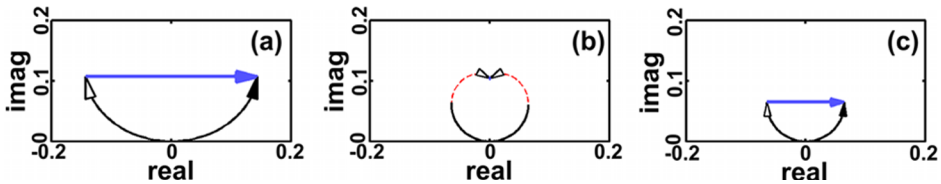


Fig. 1. (Color online) Decompositions of the OTF integral in the complex plane at spatial frequency $\|\boldsymbol{\nu}\| = 1/2$. The black and dashed red curves depict, respectively, constructive and destructive contributions $d\mathbf{u}$ to the net OTF (blue phasor), for defocus of a circular pupil for (a) $W_{20} = \lambda/4$, (b) $W_{20} = 0.642\lambda$ (for which a null occurs), and (c) with a putative mask blocking the destructive interference components yielding a positive OTF.

We can see that before renormalization by $2\pi/\Delta\varphi$, the contrast is maximized for $\Delta\varphi = \pi$ when, in the limit for large aberrations, $T = 50\%$. Following from Eq. (7), such a mask will yield approximately 20% ($2/\pi^2$) of the contrast of the diffraction-limited transfer function. More importantly, the expected MTF is independent of the magnitude of the aberrations: it is limited only by the contrast and spatial resolution of the spatial light modulator.

The same analysis can be used to derive the OTF for the binary phase masks proposed by Love *et al.* [9]. We see that this leads to an OTF equal to $4/\pi^2$ times that of the diffraction-limited MTF. Because this OTF is real and nonnegative, the maximum intensity in the image plane can be found on the optical axis. The fraction of the integral of the OTF and the integral of the diffraction-limited MTF yield a Strehl ratio of $4/\pi^2$, in agreement with that found in [9].

Only the parameters $\varphi_0$ and $\mathbf{t}$ are varied to optimize the MTF, or more specifically, the expected imaging error [16]. As we can see from the contour plot in Fig. 2, this low-dimensional optimization space contains local minima; however, our simulations indicate that a minimum very close to the global minimum can generally be achieved after only a few iterations of the differential-evolution algorithm [17], implemented in MATLAB with a population of 30, a crossover rate of 0.8, and a differential-evolution step size of 0.9.

The three masks depicted in the left column of Fig. 3 were optimized for minimum image error for three representative aberrations: astigmatism, coma, and an irregular phase aberration not atypical of the human eye [18–20]. The black areas represent opaque areas of the mask, and the hue of the transmissive areas indicates the pupil phase. The plots in the central column of Fig. 3 show the MTFs for the nonmasked, aberrated pupils: the low values and nulls in the sagittal, diagonal, and tangential MTF are readily apparent. The MTFs in the right column correspond to the masked, aberrated pupils and show a significant increase in the MTFs. Even considering that the total transmitted intensity is reduced by the mask to approximately 50%, the MTF for the masked pupil is significantly increased for all spatial frequencies and there are no nulls, thus enabling a high-quality image to be recovered.

Note that the transmission of the masks is actually larger than 50%. Although the tested aberrations are considerable, areas of the linearly changing phase exist so that the contour mask can have large open areas, such as seen at the center of Fig. 3(d). Furthermore, when at low spatial frequencies, this open area coincides with itself in the autocorrelation of the pupil function; it evokes a modest boost in the MTF as can be seen from Fig. 3(f) for spatial frequencies of $\|\nu\| \leq 1/2$.

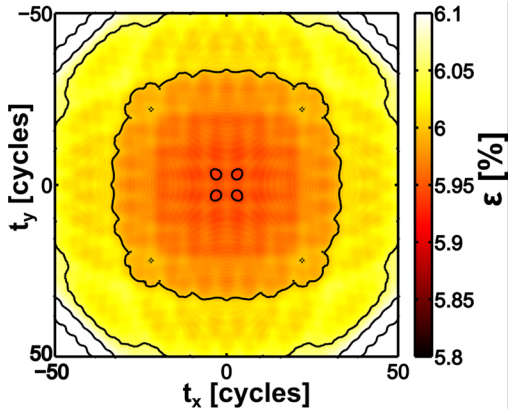


Fig. 2. (Color online) Typical cost function shown for astigmatism as a function of tip-tilt $(t_x, t_y)$, and minimized for phase reference, $\varphi_0$. Bright yellow and white regions indicate a high cost for large tip or tilt. The encircled dark red spots in the center indicate four modest tip-tilts that lead to equivalently performing masks, one of which is shown in Fig. 3(a).

### B. Contrast for a Compound Lens and Broadband Illumination

Many applications are essentially monochromatic; for instance, laser imaging, fluorescence microscopy, and retinal imaging with a scanning laser ophthalmoscope. Other applications have a modest bandwidth; e.g., true-color imaging (relative spectral width $\Delta\lambda/\lambda_0 \approx 20\%$ per channel), snapshot multiband imaging [21] (≈2%), and long-wavelength infrared imaging with quantum-well detectors (≈5%). In these cases, one might expect that mask optimization based on the above principle of monochromatic imaging might suffer some reduction in optical efficiency. As a practical example, we describe now a contour mask for enhanced off-axis imaging where the relative bandwidth is 20%.

A contour mask was optimized for correction of aberrations introduced by an $f/5$ cemented doublet when used 5° off axis at a nominal central wavelength of $\lambda_0 = 550$ nm. In this case, the aberration consists mainly of astigmatism and field curvature with a combined peak-to-valley optical path difference of approximately $10\lambda_0$. The aberration and optimized mask are shown in Fig. 4(a). MTFs calculated by ray tracing with broadband light (with wavelengths $495\,\text{nm} \leq \lambda \leq 605\,\text{nm}$, uniformly weighted) are shown in Figs. 4(b) and 4(c) respectively. We show in Figs. 4(b) that, without a mask, the MTF is strongly suppressed and contains a large number of nulls. In

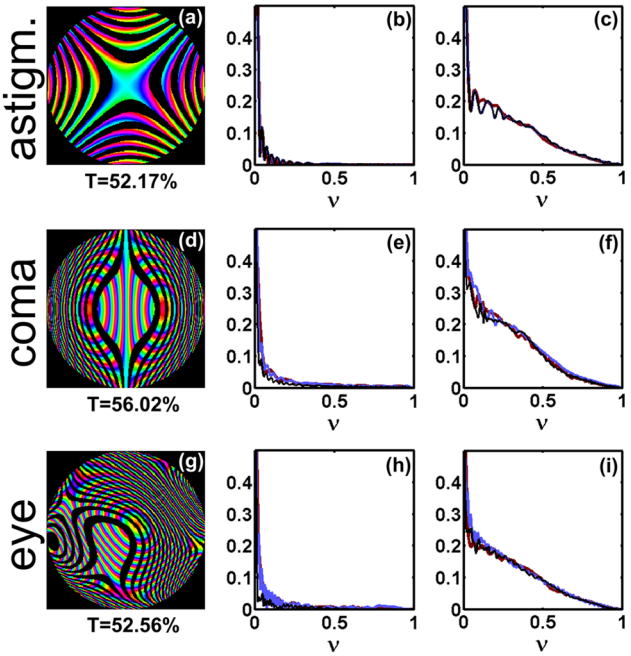


Fig. 3. (Color online) Aberration compensation of (a)–(c) astigmatism, (d)–(f) coma, and (g)–(i) an aberration representative for the human eye, of, respectively a root-mean-square optical path difference of $2\lambda$, $2\lambda$, and $3.5\lambda$. The aberration phases and contour masks with the relative transmission noted below are shown in (a), (d), and (g). The tangential (black), sagittal (blue), and diagonal (red) MTF without mask in (b), (e), and (h), and with mask in (c), (f), and (i).

4/CO 4/CO

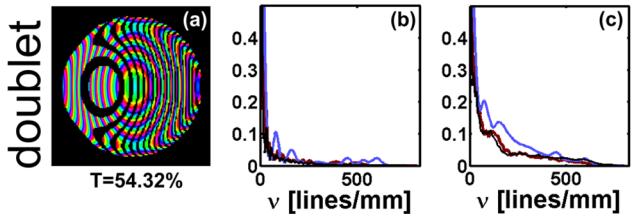


Fig. 4. (Color online) (a) Off-axis aberration at $\lambda_0 = 550\,\text{nm}$ of a cemented doublet with contour mask optimized for panchromatic operation for $495\,\text{nm} \le \lambda \le 605\,\text{nm}$ ($\Delta\lambda/\lambda_0 = 20\%$). (b) The tangential (black), sagittal (blue), and diagonal MTF (red) before and (c) after the introduction of the contour mask.

4/CO

contrast, as shown in Fig. 4(c), the addition of the mask yields a higher MTF and an absence of nulls. Although the contour mask was designed for monochromatic operation, useful aberration correction properties are maintained for a compound lens and illumination with an extended bandwidth; however, the contrast is lower than would be obtained for monochromatic operation, and although large aberrations can be corrected, the MTF will remain high only if the phase–aberration function is relatively invariant with the wavelength.

## 4. CONCLUSIONS

Binary masks can be designed to correct for phase aberrations to yield, in general, a contrast of approximately 20% ($2/\pi^2$) of the diffraction-limited MTF, and for a single spatial frequency the relative contrast can, in principle, be as high as 64% ($2/\pi$). The absence of nulls and the relatively modest reduction in the MTF allow for digital recovery of a high-quality image. Although the benefits of the masks are most pronounced for monochromatic imaging, good performance with an extended bandwidth is shown to be possible. By employing low-dimensional mask optimization (in contrast to the high-dimensional optimization proposed in [15]), binary contour masks can be calculated efficiently, facilitating their use in adaptive optics. Furthermore, adaptive programmable masks could enable image recovery for unknown aberrations following a similar approach to those currently used in conjunction with deformable mirrors [22–24].

## APPENDIX A: APPROXIMATION OF THE OPTICAL TRANSFER FUNCTION WITH A SINGLE-DIMENSIONAL INTEGRAL

The OTF defined as using the double Riemann integral of Eq. (2), can also be written using a Lebesgue integration [14], where one integrates over the possible function values $\hat{\Delta}$, of $\Delta(\mathbf{u},\boldsymbol{\nu})$ as follows:

$$\begin{aligned}\text{OTF}(\boldsymbol{\nu}) &= \frac{1}{\text{supp}(P)} \iint_{\Omega(\boldsymbol{\nu})} \exp(i\Delta(\mathbf{u},\boldsymbol{\nu}))\mathrm{d}\mathbf{u} \\ &= \frac{1}{\text{supp}(P)} \int_{-\infty}^{\infty} \exp(i\hat{\Delta})\mathrm{d}\mu(\hat{\Delta}),\end{aligned} \tag{A1}$$

with $d\mu(\hat{\Delta})$, the differential area of the integration region $\Omega(\boldsymbol{\nu})$ where $\hat{\Delta} \le \Delta(\mathbf{u},\boldsymbol{\nu}) < \hat{\Delta} + d\hat{\Delta}$.

Because $\exp(i\hat{\Delta})$ is periodic, with a period of $2\pi$, the single integral can be split into a summation of a number of intervals of size $2\pi$ covering the image of $\Delta(\mathbf{u},\boldsymbol{\nu})$:

$$\int_{-\infty}^{\infty} \exp(i\hat{\Delta})\mathrm{d}\mu(\hat{\Delta}) = \int_{-\pi}^{\pi} \exp(i\hat{\Delta}) \sum_{k=k_{\min}}^{k_{\max}} \mathrm{d}\mu(\hat{\Delta} + 2\pi k), \tag{A2}$$

where the values $k_{\min}$ and $k_{\max}$ bound the image of $\Delta(\mathbf{u},\boldsymbol{\nu})$. In other words, instead of integrating over $\hat{\Delta}$, one can integrate over $\hat{\Delta}\text{mod}2\pi$, weighting the integrand with the total area of equally spaced contours, i.e., where $\hat{\Delta} \le \Delta(\mathbf{u},\boldsymbol{\nu})\text{mod}2\pi < \hat{\Delta} + d\hat{\Delta}$.

Consider now a proportionally larger aberration with $l_c(\mathbf{u}) = c \cdot l(\mathbf{u})$, so that the difference in optical path length is correspondingly larger: $\Delta_c(\mathbf{u},\boldsymbol{\nu}) = c \cdot \Delta(\mathbf{u},\boldsymbol{\nu})$, and its area of integration $\mu_c(\hat{\Delta})$ is related as: $\mu_c(\hat{\Delta}) = \mu(\hat{\Delta}/c)$. The summation inside the integral of Eq. (A2) for the larger aberration can then be written as

$$\begin{aligned}\sum_{k=c\cdot k_{\min}}^{c\cdot k_{\max}} d\mu_c(\hat{\Delta} + 2\pi k) &= \sum_{k=c\cdot k_{\min}}^{c\cdot k_{\max}} d\mu(\hat{\Delta}/c + 2\pi k/c)1/c \\ &= \sum_{k=2\pi k_{\min}/\delta}^{2\pi k_{\max}/\delta} d\mu(\hat{\Delta}\delta/2\pi + k\delta)\delta/2\pi,\end{aligned} \tag{A3}$$

with $\delta = 2\pi/c$. Because $\hat{\Delta}$ is bound to $[-\pi,\pi]$, the term $\hat{\Delta}\delta/2\pi$ must vanish in the limit for $c \to \infty$. Hence, if the Lebesgue measure $\mu(\hat{\Delta})$ is differentiable, Eq. (A3) will converge to the integral:

$$\lim_{c\to\infty} \sum_{k=c\cdot k_{\min}}^{c\cdot k_{\max}} d\mu_c(\hat{\Delta} + 2\pi k) = \frac{1}{2\pi}\int_{-\infty}^{+\infty} \mathrm{d}\mu(\hat{\Delta})\mathrm{d}\hat{\Delta} = \frac{A_\Omega(\boldsymbol{\nu})}{2\pi}, \tag{A4}$$

with $A_\Omega(\boldsymbol{\nu})$ being the total area of the integration region. The requirement of differentiability of $\mu(\hat{\Delta})$ is not very restrictive. For the limiting cases where $\mu(\hat{\Delta})$ is not differentiable, such as for a constant $\Delta(\mathbf{u},\boldsymbol{\nu})$, the limit of Eq. (4) can be surpassed; e.g., for $\boldsymbol{\nu} = \mathbf{0}$, the OTF is unity. In general, however, for large aberrations, the phase difference $\Delta(\mathbf{u},\boldsymbol{\nu})\text{mod}2\pi$ can be considered to be uniformly distributed and the summation in Eq. (A2) can be brought outside the integral so that Eq. (3) is obtained after substitution in Eq. (A1).

## APPENDIX B: DERIVATION OF THE INDEPENDENT PUPIL APPROXIMATION TO THE OPTICAL TRANSFER FUNCTION

In general, for large aberrations, the phases $\varphi_1(\mathbf{u}) = l(\mathbf{u}-\boldsymbol{\nu})\text{mod}2\pi$ and $\varphi_2(\mathbf{u}) = l(\mathbf{u}+\boldsymbol{\nu})\text{mod}2\pi$ will also be approximately distributed uniformly. Furthermore, both variables will be independent when the phase difference $l(\mathbf{u}+\boldsymbol{\nu}) - l(\mathbf{u}-\boldsymbol{\nu})\text{mod}2\pi$ is uniformly distributed. Hence, for sufficiently large aberrations, Eq. (2) can be approximated by

$$\text{OTF}(\boldsymbol{\nu}) \approx \frac{1}{\text{supp}(P)} \int_{-\pi}^{\pi} \frac{\mathrm{d}\varphi_1}{2\pi} \iint_{\Omega(\boldsymbol{\nu})} \exp(-i\varphi_1)\exp(il(\mathbf{u}+\boldsymbol{\nu}))\mathrm{d}\mathbf{u}, \tag{A5}$$

permitting us to separate the first factor out of the internal double integral:

$$\mathrm{OTF}(\boldsymbol{\nu}) \approx \frac{1}{\mathrm{supp}(P)} \frac{1}{2\pi} \int_{-\pi}^{\pi} \exp(-i\varphi_1) \iint_{\Omega(\boldsymbol{\nu})} \times \exp(il(\mathbf{u}+\boldsymbol{\nu}))\mathrm{d}\mathbf{u}\mathrm{d}\varphi_1. \tag{A6}$$

Following the same procedure for $l(\mathbf{u}+\boldsymbol{\nu})$ as used in Appendix A for $\Delta(\mathbf{u},\boldsymbol{\nu})$, the internal double integral can be converted to a single integration:

$$\mathrm{OTF}(\boldsymbol{\nu}) \approx \frac{1}{\mathrm{supp}(P)} \frac{1}{2\pi} \int_{-\pi}^{\pi} \exp(-i\varphi_1) \frac{A_\Omega(\boldsymbol{\nu})}{2\pi} \int_{-\pi}^{+\pi} \times \exp(i\varphi_2)\mathrm{d}\varphi_2\mathrm{d}\varphi_1, \tag{A7}$$

which is equivalent to Eq. (6).

## ACKNOWLEDGMENTS

This work was funded by Qioptiq Ltd. and the Engineering and Physical Sciences Research Council (EPSRC).

## REFERENCES

1. H. Hofer, L. Chen, G.-Y. Yoon, B. Singer, Y. Yamauchi, and D. R. Williams, "Improvement in retinal image quality with dynamic correction of the eye's aberrations," Opt. Express **8**, 631–643 (2001).
2. E. J. Fernández, I. Iglesias, and P. Artal, "Closed-loop adaptive optics in the human eye," Opt. Lett. **26**, 746–748 (2001).
3. C. Paterson, I. Munro, and J. Dainty, "A low cost adaptive optics system using a membrane mirror," Opt. Express **6**, 175–185 (2000).
4. S. E. Broomfield, M. A. A. Neil, E. G. S. Paige, and G. G. Yang, "Programmable binary phase-only optical device based on ferroelectric liquid crystal SLM," Electron. Lett. **28**, 26–28 (1992).
5. K. H. Lee, J. Chang, and J. B. Yoon, "High performance microshutter device with space-division modulation," J. Micromech. Microeng. **20**, 075030 (2010).
6. S. Goodwin, B. R. Stoner, J. Carlson, and S. Rogers, "Artificial eyelid dynamic aperture optical arrays for large scale coding elements with application in the visible to MWIR," Proc. SPIE **7096**, 70960E (2008).
7. A. S. Kutyrev, R. Arendt, S. H. Moseley, R. A. Boucarut, T. Hadjimichael, M. Jhabvala, T. King, M. J. Li, J. Loughlin, D. Rapchun, D. S. Schwinger, and R. F. Silverberg, "Programmable microshutter arrays for the JWST NIRSpec: optical performance," IEEE J. Sel. Top. Quantum Electron. **10**, 652–661 (2004).
8. M. E. McNie, D. O. King, N. Price, D. J. Combes, G. W. Smith, A. G. Brown, N. T. Gordon, S. M. Stone, K. M. Brunson, K. L. Lewis, C. W. Slinger, and S. Rogers, "A large area reconfigurable MOEMS microshutter array for coded aperture imaging systems," Proc. SPIE **7096**, 70960D (2008).
9. G. D. Love, N. Andrews, P. Birch, D. Buscher, P. Doel, C. Dunlop, J. Major, R. Myers, A. Purvis, R. Sharples, A. Vick, A. Zadrozny, S. R. Restaino, and A. Glindemann, "Binary adaptive optics: atmospheric wave-front correction with a half-wave phase shifter," Appl. Opt. **34**, 6058–6066 (1995).
10. P. M. Birch, J. Gourlay, G. D. Love, and A. Purvis, "Real-time optical aberration correction with a ferroelectric liquid-crystal spatial light modulator," Appl. Opt. **37**, 2164–2169 (1998).
11. J. Osborn, R. M. Myers, and G. D. Love, "PSF halo reduction in adaptive optics using dynamic pupil masking," Opt. Express **17**, 17279–17292 (2009).
12. J. W. Goodman, *Introduction to Fourier Optics* (Roberts, 2005).
13. G. Muyo and A. R. Harvey, "Decomposition of the optical transfer function: wavefront coding imaging systems," Opt. Lett. **30**, 2715–2717 (2005).
14. A. N. Kolmogorov and S. V. Fomin, *Introductory Real Analysis* (Dover, 1975).
15. J. W. Stayman, N. Subotic, and W. Buller, "An analysis of coded aperture acquisition and reconstruction using multi-frame code sequences for relaxed optical design constraints," Proc. SPIE **7468**, 74680D (2009).
16. T. Vettenburg, N. Bustin, and A. R. Harvey, "Fidelity optimization for aberration-tolerant hybrid imaging systems," Opt. Express **18**, 9220–9228 (2010).
17. R. Storn and K. Price, "Differential evolution—a simple and efficient heuristic for global optimization over continuous spaces," J. Global Optim. **11**, 341–359 (1997).
18. J. Porter, A. Guirao, I. G. Cox, and D. R. Williams, "Monochromatic aberrations of the human eye in a large population," J. Opt. Soc. Am. A **18**, 1793–1803 (2001).
19. A. Guirao, M. Redondo, and P. Artal, "Optical aberrations of the human cornea as a function of age," J. Opt. Soc. Am. A **17**, 1697–1702 (2000).
20. C. Torti, S. Gruppetta, and L. Diaz-santana, "Wavefront curvature sensing for the human eye," J. Modern Opt. **55**, 691–702 (2008).
21. A. Gorman, D. W. Fletcher-Holmes, and A. R. Harvey, "Generalization of the Lyot filter and its application to snapshot spectral imaging," Opt. Express **18**, 5602–5608 (2010).
22. R. A. Muller and A. Buffington, "Real-time correction of atmospherically degraded telescope images through image sharpening," J. Opt. Soc. Am. **64**, 1200–1210 (1974).
23. A. Buffington, F. S. Crawford, R. A. Muller, A. J. Schwemin, and R. G. Smits, "Correction of atmospheric distortion with an image-sharpening telescope," J. Opt. Soc. Am. **67**, 298–303 (1977).
24. D. Débarre, M. J. Booth, and T. Wilson, "Image based adaptive optics through optimisation of low spatial frequencies," Opt. Express **15**, 8176–8190 (2007).

# Queries

1. Are there specific contract numbers related to the financial support?